Time integration scheme for elastoplastic models based on anisotropic strain-rate potentials

Meziane Rabahallah, Tudor Balan, Salima Bouvier, Cristian Teodosiu

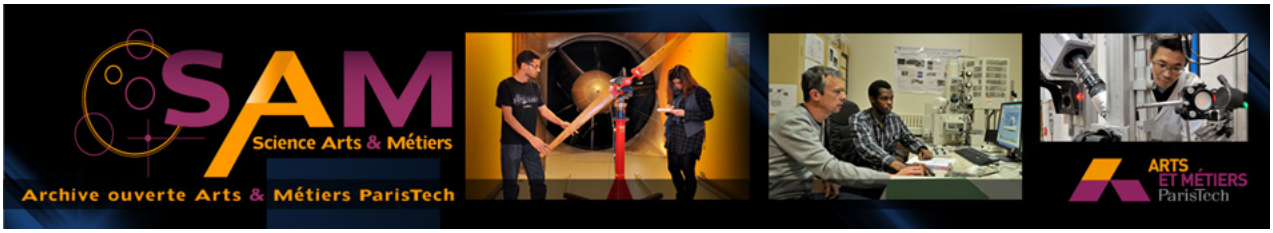

Time integration scheme for elastoplastic models based on anisotropic strain-rate potentials

MEZIANE RABAHALLAH[1,2], TUDOR BALAN[1,*,†], SALIMA BOUVIER[2], CRISTIAN TEODOSIU[2]

[1] *LPMM-CNRS, Arts et Métiers ParisTech – Metz Campus, 4 rue A. Fresnel, 57078 Metz Cedex 03, France*
[2] *LPMTM-CNRS, Université Paris 13, Institut Galilée, 99 rue J.-B. Clément, 93430 Villetaneuse, France*

SUMMARY

Modelling of plastic anisotropy requires the definition of stress potentials (coinciding with the yield criteria in case of the associated flow rules) or, alternatively, plastic strain-rate potentials. The latter approach has several advantages whenever material parameters are determined by means of texture measurements and crystal plasticity simulations. This paper deals with a phenomenological description of anisotropy in elastoplastic rate-insensitive models, by using strain-rate potentials. A fully implicit time integration algorithm is developed in this framework and implemented in a static-implicit finite element code. Algorithmic details are discussed, including the derivation of the consistent (algorithmic) tangent modulus and the numerical treatment of the yield condition. Typical sheet-forming applications are simulated with the proposed implementation, using the recent non-quadratic strain-rate potential Srp2004-18p. Numerical simulations are carried out for materials that exhibit strong plastic anisotropy. The numerical results confirm that the presented algorithm exhibits the same generality, robustness, accuracy, and time-efficiency as state-of-the-art yield-criterion-based algorithms.

KEY WORDS: stress update algorithm; backward Euler; plastic strain-rate potential; elastoplasticity; sheet metal forming simulation.

[*] Correspondence to: Tudor Balan, Arts et Métiers ParisTech – Metz Campus, 4 rue A. Fresnel, 57078 Metz Cedex 03, France
[†] E-mail: tudor.balan@ensam.fr.

1 INTRODUCTION

The description of plastic anisotropy is recognized as a key factor for the accuracy of finite element simulations of sheet metal forming processes. This is particularly true when final part properties, such as springback or forming limits, are to be investigated. The initial plastic anisotropy of metal sheets is classically modelled either by micromechanics or phenomenological yield criteria, the latter being preferred whenever numerical simulations are performed. In order to phenomenologically represent the rate-insensitive, incompressible plastic behaviour of materials, classical constitutive models use a yield function (for a yield surface description), the associated flow (or normality) rule, and a hardening law. The first two express anisotropic relationships between the stress and plastic strain rate components at a given material point.

Ziegler [1] and Hill [2] have shown that, based on the plastic work equivalence principle, a meaningful strain rate potential can be associated with any convex stress potential (or yield surface). Therefore, an alternative approach to describing plastic anisotropy is to provide a strain rate potential, which is expressed as a function of the plastic strain rate tensor, while its gradient gives the direction of the stress deviator. Arminjon et al. [3, 4] and Van Houtte *et al.* [5] proposed fourth-order and sixth-order strain rate functions, respectively. Barlat and Chung [6], Barlat *et al.* [7], Chung *et al.* [8], and Kim *et al.* [9] introduced strain-rate potentials that were pseudo-conjugates of yield functions published earlier.

Formally, the stress or strain-rate potential approaches are identical. A strong driving force for the development of strain-rate potentials has been their convenient parameter identification by means of micro-mechanical calculations based on Taylor-type models [3, 5]. For some applications, such as rigid-plastic finite element (FE) simulations [10-12], minimum plastic-work path calculations [7], inverse one-step analysis [13], and analytical calculations in material forming, the strain-rate potential approach can be computationally more convenient. Nevertheless, numerical implementation of strain-rate potentials has been also tackled in the framework of elastoplasticity. In their finite element implementation, Bacroix and Gilormini [14] proposed a solution to overcome the lack of an explicit yield condition in this modelling framework. They used a finite-difference tangent modulus and membrane elements to simulate a simplified cup drawing process. A method used to derive the algorithmic tangent modulus for strain-rate-potential-based elastoplastic models has been proposed by Szabo and Jonas [15]. Van Houtte et al. [16], Hoferlin et al. [17], and Li et al. [18, 19] developed implicit FE implementations and performed sheet forming simulations with their sixth-order plastic potential [5]; Zhou et al. [20, 21] implemented similar fourth-order [4] and sixth-order [22] potentials; Kim et al. [23] recently proposed a general plane-stress finite element implementation for use with shell elements.

One can note, however, that most of the former computer implementations have been designed with feasibility in mind, rather than generality. They were developed for specific strain-rate potentials, e.g., those involving complex numerical treatments to deal with convexity issues;

hardening models were either oversimplified [14, 20, 21] or very specific [19], with microstructural and textural relevance being the main objectives. These developments have been conducted in the context of texture-based parameter identification, and hence the materials science background has been taken into account throughout the development of the numerical scheme. A complete minimization technique has been developed and used to determine the intersection of the trial stress increment with the yield surface, which is not really a requirement for the return mapping algorithm.

On the other hand, strain-rate potentials have been originally proposed for specific applications, whereas yield criteria were considered better suited for the elastoplastic FE implementation. Today, however, flexible strain-rate potentials have been proposed that exhibit excellent predictive abilities for general application [24]. Thus, the availability of strain-rate potentials in finite element codes would bring a real added value to the sheet metal forming community, both in research work and industrial applications.

The aim of this paper is to propose a generic implicit time integration algorithm for anisotropic elastoplastic, time-independent constitutive models using the strain-rate potential approach. Compared to the state-of-the-art integration schemes developed for yield criteria, the proposed algorithm is expected to exhibit the same generality, robustness, accuracy, and time-efficiency. Existing rigid-plastic FE implementations prevent the use of strain-rate potentials for sheet forming simulations including unloading and springback.

The structure of the paper is as follows. The strain-rate potential-based elastoplastic modelling framework is briefly presented in Section 2. Section 3 is devoted to the development of the implicit time integration algorithm, which is presented in detail and kept as general and complete as possible. In Section 4, the quadratic Hill potential, as well as the recent, non-quadratic potential Srp2004-18p are taken as particular cases of strain-rate potentials, together with a non-linear isotropic-kinematic hardening model. The resulting algorithm is implemented into the software Abaqus/Standard. Validation and comparison with pseudo-conjugate yield criteria are performed through numerical simulations of typical sheet metal forming processes.

2 CONSTITUTIVE MODEL

The phenomenological elastoplastic modelling adopted here is rate independent (without viscous effects) and restricted to cold deformation. Classical rate-independent models utilize a hypo-elastic law defining the stress rate with respect to the elastic strain rate, a yield function delimiting the elastic zone, a plastic flow rule, and a set of internal state variable evolution laws defining the work hardening during plastic deformation. In the current setting, the yield function is replaced by a plastic strain-rate potential and the flow rule is modified accordingly. The frame objectivity issue, which arises when large deformations are intended, is solved by writing the constitutive equations in an appropriate rotating orthogonal frame.

Vector and tensor variables are denoted by bold-face symbols. Components, whenever used, are referred to a Cartesian orthogonal frame. The summation convention over repeated indices of

such components is used throughout the paper. Let **A**, **B** denote second-order tensors and **C** a fourth-order tensor. The double-contracted tensor products between such tensors are defined as:

$$\mathbf{A}:\mathbf{B} = A_{ij}B_{ij}, \quad (\mathbf{C}:\mathbf{A})_{ij} = C_{ijkl}A_{kl}, \quad \mathbf{A}:\mathbf{C}:\mathbf{B} = A_{ij}C_{ijkl}A_{kl} \tag{1}$$

The norm of **A** is defined as $\|\mathbf{A}\| = \sqrt{\mathbf{A}:\mathbf{A}}$, and its direction, if **A** is non-zero, as $\mathbf{A}/\|\mathbf{A}\|$. The norm of **C** is defined by $\|\mathbf{C}\| = \sqrt{C_{ijkl}C_{ijkl}}$. Finally, $(\mathbf{A}\otimes\mathbf{B})_{ijkl} = A_{ij}B_{kl}$. Note that all second- and fourth-order tensors that enter the modelling described hereafter are supposed fully symmetric.

2.1 Rotation-compensated tensor quantities and equations

The sheet undergoes generally large deformations in metal forming and its elastoplastic behaviour is described by rate constitutive equations. In order to achieve material objectivity, objective rates must be used. A very convenient approach used to ensure material objectivity, while keeping the constitutive equation simple in form, consists of reformulating these equations in terms of rotation-compensated variables. More precisely, if **A** and **C** designate second- and fourth-order tensors, respectively, the corresponding rotation-compensated tensors (labelled by a superposed hat) re defined by

$$\hat{A}_{ij} = \mathfrak{R}_{ki}\mathfrak{R}_{lj}A_{kl}, \qquad \hat{C}_{ijkl} = \mathfrak{R}_{pi}\mathfrak{R}_{qj}\mathfrak{R}_{rk}\mathfrak{R}_{sl}C_{pqrs}, \tag{2}$$

where $\mathfrak{R}$ is an orthogonal rotation matrix, generated by a skew-symmetric spin tensor $\mathbf{\Omega}$ using $\dot{\mathfrak{R}}\cdot\mathfrak{R}^T = \mathbf{\Omega}$, where the superposed dot on $\mathfrak{R}$ denotes time differentiation and the superscript T indicates the transpose of $\mathfrak{R}$.

The main interest of this approach is that objective derivatives (labelled here by a superposed circle) are simply related to the material time derivatives of their rotation-compensated counterparts via equations similar to Eq. (2), *i.e.,*

$$\dot{\hat{A}}_{ij} = \mathfrak{R}_{ki}\mathfrak{R}_{lj}\overset{\circ}{A}_{kl}, \qquad \dot{\hat{C}}_{ijkl} = \mathfrak{R}_{pi}\mathfrak{R}_{qj}\mathfrak{R}_{rk}\mathfrak{R}_{sl}\overset{\circ}{C}_{pqrs} \tag{3}$$

Clearly, $\mathfrak{R}$ should satisfy, in turn, the objectivity condition under superimposed rigid-body motions. For example, the Jaumann derivative is obtained by setting $\mathbf{\Omega} = \mathbf{W}$, while using $\mathfrak{R} = \mathbf{R}$ leads to the Green-Naghdi derivative. Here **W** denotes the total spin, while **R** is the orthogonal tensor in the polar decomposition of the deformation gradient. It should be noted that, following Mandel's pioneering work on the average plastic spin of polycrystals [25], other phenomenological models have been proposed to describe the evolution of the plastic spin (see, e.g., [26-28]), and their computer implementation has also been studied [29, 30].

In the following, we assume throughout that all tensor variables turn with the spin **W** (i.e., Jaumann rates are considered), and that they are rotation-compensated. Consequently, simple

time derivatives are involved in the constitutive equations, making them identical in form to a small-strain formulation. For simplicity, the superposed hat (^) is omitted thereafter.

2.2 Modelling framework

The total strain rate tensor $\mathbf{D}$ is decomposed into an elastic part $\mathbf{D}^e$ and a plastic part $\mathbf{D}^p$:

$$\mathbf{D} = \mathbf{D}^e + \mathbf{D}^p \tag{4}$$

and, therefore, the linear, hypoelastic response of the material is described by

$$\dot{\boldsymbol{\sigma}} = \mathbf{C}^e : \left(\mathbf{D} - \mathbf{D}^p\right), \tag{5}$$

where $\dot{\boldsymbol{\sigma}}$ is the rate of the Cauchy stress tensor $\boldsymbol{\sigma}$ and $\mathbf{C}^e$ is the fourth-order elasticity tensor. In the case of isotropic linear elasticity, $\mathbf{C}^e = 2G\,\mathbf{I}_4^{'s} + K\,\mathbf{I}\otimes\mathbf{I}$, with K and G being the bulk and shear moduli, respectively. Finally, $\mathbf{I}$ is the unit second-order tensor, whose components are the Kronecker's deltas, i.e. $I_{kl} = \delta_{kl}$, while $\mathbf{I}_4^{'s}$ is the fourth-order symmetric deviatoric unit tensor, whose components are $I'^{s}_{4ijkl} = (1/2)(\delta_{ik}\delta_{jl} + \delta_{il}\delta_{jk}) - (1/3)\delta_{ij}\delta_{kl}$.

In associated rate-independent incompressible plasticity, the plastic strain rate tensor $\mathbf{D}^p$ is supposed proportional to the gradient of a yield function Φ, defined as

$$\Phi\left(\boldsymbol{\sigma}, \tau, \mathbf{X}\right) = \bar{\sigma}\left(\boldsymbol{\sigma} - \mathbf{X}\right) - \tau = 0. \tag{6}$$

Here, the scalar variable τ is a measure of the "size" of the elastic domain (and describes the isotropic hardening), $\mathbf{X}$ locates the "centre" of this elastic domain in the stress space (and introduces the kinematic hardening), and $\bar{\sigma}$ is the equivalent stress defining its shape. The flow rule reads

$$\mathbf{D}^P = \dot{\lambda}\frac{\partial\Phi\left(\boldsymbol{\sigma}, \tau, \mathbf{X}\right)}{\partial\boldsymbol{\sigma}}, \tag{7}$$

where $\dot{\lambda}$ is the plastic multiplier, which is supposed strictly positive for plastic loading, and equal to zero for neutral plastic loading, for unloading, and in elastic state.

In the current work, the dual potential Ψ of the yield function Φ is used instead:

$$\Psi(\mathbf{D}^p) = \dot{\lambda}. \tag{8}$$

The flow rule becomes

$$\mathbf{T} = \tau \frac{\partial \Psi}{\partial \mathbf{D}^p}, \tag{9}$$

where $\mathbf{T} = \boldsymbol{\sigma}' - \mathbf{X}$ is the effective stress tensor and $\boldsymbol{\sigma}'$ denotes the deviator of the stress tensor $\boldsymbol{\sigma}$. In this work, we restrict ourselves to functions Ψ and Φ that are first-order homogeneous with respect to positive scalar multipliers. Although the existence of dual potentials is theoretically demonstrated, the analytical expression of a strain-rate potential is seldom calculated as the dual of a given yield function.

The two hardening variables τ and $\mathbf{X}$ evolve with the plastic strain. Their evolution equations are sought in the generic form

$$\dot{\mathbf{X}} = \mathbf{h}_X \dot{\lambda}, \qquad \dot{\tau} = h_\tau \dot{\lambda}. \tag{10}$$

Note again that objective rates must be used in Eq. (5) and (10), should the model be written in a fixed frame rather than the particular rotating frame adopted here.

By using the consistency condition for plastic loading, the following linear tangent relation can be derived between the stress rate and the strain rate tensors

$$\dot{\boldsymbol{\sigma}} = \mathbf{C}^{ana} : \mathbf{D}, \tag{11}$$

where the analytical tangent modulus $\mathbf{C}^{ana}$ takes the form [31]

$$\mathbf{C}^{ana} = \mathbf{C}^e - \alpha \frac{\left(\mathbf{C}^e : \mathbf{N}\right) \otimes \left(\mathbf{N} : \mathbf{C}^e\right)}{\mathbf{N} : \mathbf{C}^e : \mathbf{N} + \left(\mathbf{N} : \mathbf{h}_X + \Psi(\mathbf{N}) h_\tau\right) \Psi(\mathbf{N})}, \tag{12}$$

with $\alpha = 1$ for plastic loading and $\alpha = 0$ otherwise; $\mathbf{N} = \mathbf{D}^p / \| \mathbf{D}^p \|$ denotes the plastic strain rate direction. When the elasticity is linear and isotropic, this relation reduces further to

$$\mathbf{C}^{ana} = K \mathbf{I} \otimes \mathbf{I} + 2G \mathbf{I}_4^{'s} - \alpha \frac{4G^2 \mathbf{N} \otimes \mathbf{N}}{2G + \left(\mathbf{N} : \mathbf{h}_X + \Psi(\mathbf{N}) h_\tau\right) \Psi(\mathbf{N})}. \tag{13}$$

3 TIME INTEGRATION ALGORITHM

The elastoplastic model introduced in Section 2 has been implemented in the static implicit code ABAQUS/Standard. At each equilibrium iteration, a displacement increment is predicted in each node of the mesh. From this, the kinematic equations are employed to calculate the strain increment at each integration point of the finite elements. These steps are carried out by the FE code, so only the update of the state variables needs to be performed in order to verify the

equilibrium at the end of the loading increment. In this section, we develop the state update methodology and derive the consistent tangent modulus necessary to iteratively reach the equilibrium at the end of each loading increment.

The total and plastic strain increments $\Delta\boldsymbol{\varepsilon}$ and $\Delta\boldsymbol{\varepsilon}^p$ are defined as

$$\Delta\boldsymbol{\varepsilon} = \int_{t_n}^{t_{n+1}} \mathbf{D}\ \mathrm{dt}, \qquad \Delta\boldsymbol{\varepsilon}^p = \int_{t_n}^{t_{n+1}} \mathbf{D}^p\ \mathrm{dt} \tag{14}$$

and must be further approximated since the values of $\mathbf{D}$ and $\mathbf{D}^p$ are only available at the two ends of the time increment $\Delta t = t_{n+1} - t_n$. Several approximations for the strain increment have been proposed in the literature and they are already implemented in the finite element codes, as the strain increment is an input variable for the constitutive algorithm. For the plastic strain increment, the backward Euler time integration scheme assumes that $\mathbf{D}^p$ is constant over the increment and equal to its value at t_{n+1}, i.e.

$$\Delta\boldsymbol{\varepsilon}^p \approx \mathbf{D}^p_{n+1}\Delta t. \tag{15}$$

As a consequence, due to the first-order homogeneity of the plastic potential with respect to scalar multipliers, one can write the incremental form of Eq. (8) in any of the following equivalent forms:

$$\Delta\lambda = \Psi(\Delta\boldsymbol{\varepsilon}^p) = (\Delta\mathrm{t})\,\Psi(\mathbf{D}^p_{n+1}) = (\Delta\mathrm{t})\left\|\mathbf{D}^p_{n+1}\right\|\Psi(\mathbf{N}_{n+1}) = \left\|\Delta\boldsymbol{\varepsilon}^p\right\|\Psi(\mathbf{N}_{n+1}), \tag{16}$$

where the direction of the plastic strain rate at the end of the increment can be written as

$$\mathbf{N}_{n+1} = \frac{\mathbf{D}^p_{n+1}}{\left\|\mathbf{D}^p_{n+1}\right\|} = \frac{\Delta\boldsymbol{\varepsilon}^p}{\left\|\Delta\boldsymbol{\varepsilon}^p\right\|} \tag{17}$$

The derivatives of the plastic potential can also take different equivalent forms, which can prove to be useful in particular contexts:

$$\boldsymbol{\xi} = \frac{\partial\Psi\left(\mathbf{D}^p_{n+1}\right)}{\partial\mathbf{D}^p_{n+1}} = \frac{\partial\Psi\left(\Delta\boldsymbol{\varepsilon}^p\right)}{\partial\left(\Delta\boldsymbol{\varepsilon}^p\right)} = \frac{\partial\Psi\left(\mathbf{N}_{n+1}\right)}{\partial\mathbf{N}_{n+1}}. \tag{18}$$

Equations (16) and (18) show that the effects of the norm $\left\|\Delta\boldsymbol{\varepsilon}^p\right\|$ and the direction $\mathbf{N}_{n+1}$ of the plastic strain increment can be separated. This observation may be used at the algorithmic level to locally reduce the number of unknowns.

3.1 Discrete equations of the constitutive model

In the previous section, Eqs. (5) and (8)-(10) were shown to completely define the constitutive model. The FE implementation of such a model requires the numerical integration of these equations over a time increment, from a known state at time t_n to the unknown state at t_{n+1}, given the total strain increment $\Delta\boldsymbol{\varepsilon}$. The most widely used method is the fully implicit, backward Euler integration scheme (see, e.g., [32-34]), which is also employed in this work.

The incremental form of the hypoelastic Hooke's law is written as

$$\boldsymbol{\sigma}_{n+1} = \boldsymbol{\sigma}_n + \mathbf{C}^e : \left(\Delta\boldsymbol{\varepsilon} - \Delta\boldsymbol{\varepsilon}^p\right). \tag{19}$$

The implicit time integration schemes of rate-independent plasticity models include an elastic trial $\boldsymbol{\sigma}^{try} = \boldsymbol{\sigma}_n + \mathbf{C}^e : \Delta\boldsymbol{\varepsilon}$ followed, when necessary, by a plastic correction. This two-step procedure is illustrated in Figure 1, together with some of the notation used in this section. The decision about whether the trial stress corresponds to an elastic state or an elastoplastic one requires a particular attention here since, in the framework of strain-rate potentials, no explicit yield criterion is available. This issue will be clarified in Section 3.2.

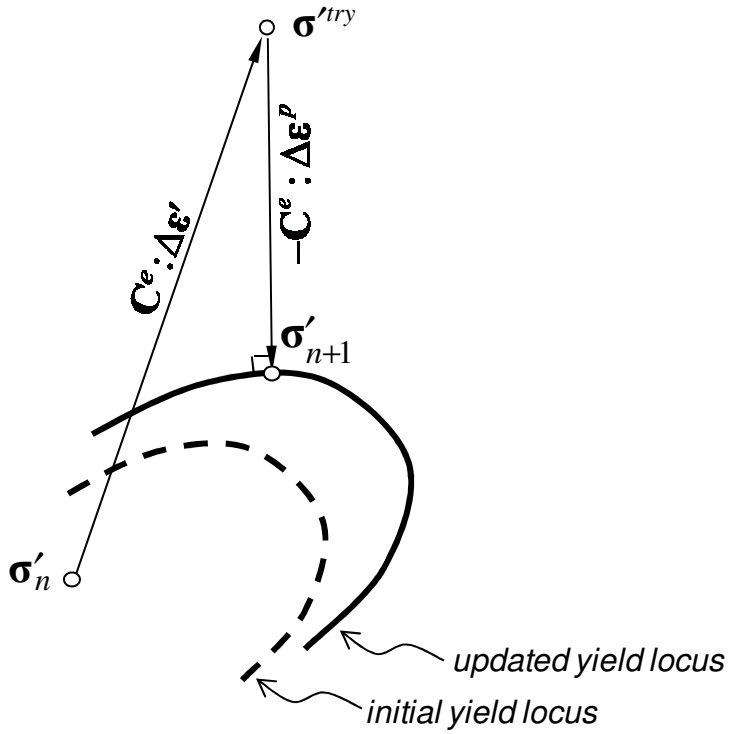

Figure 1. Elastic prediction and plastic correction during a typical elastoplastic increment; graphical illustration in the deviatoric stress space.

The elastic trial stress $\boldsymbol{\sigma}^{try}$ can be computed explicitly since the total strain increment is known at the beginning of the time step, together with the spherical (hydrostatic) part of the final stress

$$\boldsymbol{\sigma}_{n+1}^{sph} = (1/3)\, tr\left(\boldsymbol{\sigma}_{n+1}\right)\mathbf{I} = (1/3)\, tr\left(\boldsymbol{\sigma}_{n}\right)\mathbf{I} + K\, tr\left(\Delta\boldsymbol{\varepsilon}\right)\mathbf{I} \tag{20}$$

since it also depends only on known quantities. However, the deviatoric part of the final stress depends on the yet unknown increment of plastic strain, since

$$\boldsymbol{\sigma}'_{n+1} = \boldsymbol{\sigma}'_{n} + \mathbf{C}^{e} : \left(\Delta\boldsymbol{\varepsilon}' - \Delta\boldsymbol{\varepsilon}^{p}\right). \tag{21}$$

An alternative way of computing the deviatoric stress at the end of the increment is provided by the incremental form of Eq. (9):

$$\boldsymbol{\sigma}'_{n+1} = \mathbf{X}_{n+1} + \tau_{n+1}\frac{\partial\Psi}{\partial(\Delta\boldsymbol{\varepsilon}^{p})}. \tag{22}$$

Combining Eqs. (21) and (22) yields the following nonlinear system of algebraic equations:

$$\mathbf{X}_{n+1} + \tau_{n+1}\frac{\partial\Psi}{\partial(\Delta\boldsymbol{\varepsilon}^{p})} - \mathbf{C}^{e} : \left(\Delta\boldsymbol{\varepsilon}' - \Delta\boldsymbol{\varepsilon}^{p}\right) - \boldsymbol{\sigma}'_{n} = \mathbf{0}. \tag{23}$$

Consequently, the time integration problem of the constitutive model is reduced to solving this system[1], the principal unknown being $\Delta\boldsymbol{\varepsilon}^{p}$. Then, the updated stress is computed as

$$\boldsymbol{\sigma}_{n+1} = \boldsymbol{\sigma}'_{n+1} + \boldsymbol{\sigma}_{n+1}^{sph}. \tag{24}$$

For the Newton-Raphson solution of Eq. (23), one defines the residual function $\boldsymbol{\rho}(\Delta\boldsymbol{\varepsilon}^{p})$ as

$$\boldsymbol{\rho}\left(\Delta\boldsymbol{\varepsilon}^{p}\right) = \mathbf{X}_{n+1} + \tau_{n+1}\frac{\partial\Psi(\Delta\boldsymbol{\varepsilon}^{p})}{\partial(\Delta\boldsymbol{\varepsilon}^{p})} - \mathbf{C}^{e} : \left(\Delta\boldsymbol{\varepsilon}' - \Delta\boldsymbol{\varepsilon}^{p}\right) - \boldsymbol{\sigma}'_{n} = \mathbf{0}. \tag{25}$$

An initial value $\Delta\boldsymbol{\varepsilon}_{(0)}^{p}$ for the plastic strain increment is calculated and then corrected at each iteration "*k*" with the correction term

$$\delta\Delta\boldsymbol{\varepsilon}_{(k+1)}^{p} = -\left[\frac{\partial\boldsymbol{\rho}\left(\Delta\boldsymbol{\varepsilon}_{(k)}^{p}\right)}{\partial\Delta\boldsymbol{\varepsilon}^{p}}\right]^{-1} : \boldsymbol{\rho}\left(\Delta\boldsymbol{\varepsilon}_{(k)}^{p}\right) \tag{26}$$

The Jacobian $\partial\boldsymbol{\rho}/\partial(\Delta\boldsymbol{\varepsilon}^{p})$ is calculated by differentiation of Eq. (25):

$$\frac{\partial\boldsymbol{\rho}(\Delta\boldsymbol{\varepsilon}^{p})}{\partial(\Delta\boldsymbol{\varepsilon}^{p})} = \frac{\partial\mathbf{X}}{\partial(\Delta\boldsymbol{\varepsilon}^{p})} + \frac{\partial\Psi(\Delta\boldsymbol{\varepsilon}^{p})}{\partial(\Delta\boldsymbol{\varepsilon}^{p})} \otimes \frac{\partial\tau}{\partial(\Delta\boldsymbol{\varepsilon}^{p})} + \tau\frac{\partial^{2}\Psi(\Delta\boldsymbol{\varepsilon}^{p})}{\partial^{2}(\Delta\boldsymbol{\varepsilon}^{p})} + \mathbf{C}^{e} : \mathbf{I}_{4}^{'s}. \tag{27}$$

[1] It is implicitly assumed here that each of the state variables τ_{n+1} and $\mathbf{X}_{n+1}$ can be explicitly written in terms of $\Delta\boldsymbol{\varepsilon}^{p}$. This assumption is easily verified for the combined isotropic-kinematic model used in section 4.1; it has also been shown [19, 35] to be true for the much more complex model of Teodosiu and Hu [36].

The solution of Eq. (25) requires the calculation of the plastic potential and of its first- and second-order derivatives:

$$\Delta\lambda = \Psi(\Delta\boldsymbol{\varepsilon}^p), \qquad \boldsymbol{\xi} = \frac{\partial\Psi(\Delta\boldsymbol{\varepsilon}^p)}{\partial(\Delta\boldsymbol{\varepsilon}^p)}, \qquad \boldsymbol{\zeta} = \frac{\partial^2\Psi(\Delta\boldsymbol{\varepsilon}^p)}{\partial^2(\Delta\boldsymbol{\varepsilon}^p)}, \tag{28}$$

as well as the values of the internal variables τ_{n+1} and $\mathbf{X}_{n+1}$ and of their first-order derivatives $\partial\tau/\partial(\Delta\boldsymbol{\varepsilon}^p)$ and $\partial\mathbf{X}/\partial(\Delta\boldsymbol{\varepsilon}^p)$. These terms are the only ones specific to the particular forms of the anisotropy and hardening models; some examples are given in Section 4. The rest of the procedure is general and can be used with any other model.

3.2 Yield condition

In classical rate-independent plasticity, the elastic trial stress is used to evaluate the yield function. If the yield condition is not verified (nor violated), then the increment is elastic and $\boldsymbol{\sigma}_{n+1} = \boldsymbol{\sigma}^{try}$; otherwise, the plastic correction should be applied. In the present case, no explicit yield condition is available. To overcome this difficulty, Bacroix and Gilormini [14, 37] have developed a strain-rate-potential-based yield condition, using the following function of the plastic strain rate direction:

$$g(\mathbf{N}) = \tau\Psi(\mathbf{N}) - \mathbf{T}:\mathbf{N}. \tag{29}$$

Based on the maximum work principle, the authors have shown that for a given stress state, a yield condition can be written as:

$$\underset{\mathbf{N}}{\mathrm{Min}}\left[\tau\Psi(\mathbf{N}) - \mathbf{T}:\mathbf{N}\right] \begin{cases} <0 & \text{if } \boldsymbol{\sigma} \text{ lays outside the yield surface,} \\ =0 & \text{if } \boldsymbol{\sigma} \text{ lays on the yield surface,} \\ >0 & \text{if } \boldsymbol{\sigma} \text{ lays inside the yield surface.} \end{cases} \tag{30}$$

Four independent angles θ_1, θ_2, θ_3, and θ_4 are used to define the components of the unit-length tensor **N**, their collection being denoted by $\boldsymbol{\theta}$. This compact notation is described in more detail in the Appendix. The minimization of *g* with respect to $\boldsymbol{\theta}$ is associated to the solution of the following equation:

$$\frac{\partial g(\boldsymbol{\theta})}{\partial\boldsymbol{\theta}} = \mathbf{0}, \tag{31}$$

where

$$\frac{\partial g(\boldsymbol{\theta})}{\partial\boldsymbol{\theta}} = \tau\left[\frac{\partial\Psi(\mathbf{N})}{\partial\mathbf{N}} - \frac{\mathbf{T}}{\tau}\right] : \frac{\partial\mathbf{N}}{\partial\boldsymbol{\theta}}. \tag{32}$$

The BFGS minimization algorithm is used in order to avoid analytical calculation of the Hessian $\partial^2 g(\boldsymbol{\theta})/\partial^2 \boldsymbol{\theta}$, which is instead approximated numerically. The BFGS algorithm has also the advantage of providing a better convergence whenever the initial guess is far from the solution or the function *g* is not proven to be convex.

In Eq. (32), the term $\partial \Psi(\mathbf{N})/\partial \mathbf{N}$ depends on the chosen potential, while $\partial \mathbf{N}/\partial \boldsymbol{\theta}$ depends only on the definition (56) and is computed once for all as

$$\frac{\partial \mathbf{N}}{\partial \boldsymbol{\theta}} = \begin{bmatrix} -s_1 s_2 s_3 s_4 & c_1 c_2 s_3 s_4 & c_1 s_2 c_3 s_4 & c_1 s_2 s_3 c_4 \\ c_1 s_2 s_3 s_4 & s_1 c_2 s_3 s_4 & s_1 s_2 c_3 s_4 & s_1 s_2 s_3 c_4 \\ 0 & -s_2 s_3 s_4 & c_2 c_3 s_4 & c_2 s_3 c_4 \\ 0 & 0 & -s_3 s_4 & c_3 c_4 \\ 0 & 0 & 0 & -s_4 \end{bmatrix}, \tag{33}$$

where $c_i = \cos\theta_i$ and $s_i = \sin\theta_i$; $i = \overline{1,4}$.

As compared to the classical elastoplastic models, the verification of the yield condition seems more expensive here, since a minimization problem has to be solved. In practice, this extra cost can be avoided in most cases. As underlined by Hoferlin [38], the trial stress is surely elastic and no check needs to be made whenever the deviatoric effective trial stress $\boldsymbol{\sigma}'^{try} - \mathbf{X}_n$ is much smaller than τ_n, e.g.,

$$\left\| \boldsymbol{\sigma}'^{try} - \mathbf{X} \right\| / \tau \le 0.1 \tag{34}$$

When the initial stress $\boldsymbol{\sigma}_n$ lies on the yield surface, the following simple condition guarantees that the trial stress lies outside the yield surface [32], and hence that the increment is elastoplastic:

$$\left(\boldsymbol{\sigma}'^{try} - \boldsymbol{\sigma}'_n \right) : \mathbf{N}_n \ge 0 , \tag{35}$$

where $\mathbf{N}_n$ is the normal to the initial yield surface, which can be stored at each increment for future use. The use of Eq. (35) renders the minimization unnecessary in most situations. Finally, in the remaining cases, when the minimization must be performed, it can be stopped as soon as a tensor **N** is found so that $g(\mathbf{N})<0$. Indeed, the minimum is guaranteed to be negative in this case, so the increment is elastoplastic. Note that the plastic strain rate direction **N** that minimizes $g(\mathbf{N})$ in Eq. (30) has no relevance with respect to the solution of Eq. (25). Consequently, there is no need to calculate its exact value. In practice, several simple initializations for **N** already fulfil this condition in most cases. Thus, the minimization procedure seldom needs more than

one iteration, which is equivalent to the classical yield condition in terms of computational cost. These conjectures will be further substantiated in Section 4.

3.3 Consistent tangent modulus

The user material routine in a finite element code must update the stress (and other state variables) over a strain increment, and it must also provide the modulus defining the tangent relation between the stress increment and the strain increment. This so-called algorithmic (or consistent) tangent modulus $\mathbf{C}^{alg}$ is required for the finite element equilibrium iterations. In the framework of strain-rate potentials, algorithmic tangent moduli have been derived by Bird and Martin [39] in the case of elastic-perfectly plastic materials, by Szabó and Jonas [15] for isotropic hardening, and by Hoferlin [38] for combined nonlinear isotropic-kinematic hardening models. The last modulus can be applied for the present model; its expression reads

$$D\boldsymbol{\sigma}_{n+1} = \left[\left(\mathbf{C}^{e} \right)^{-1} + \mathbf{I}_4^{\prime s} : \left(\mathbf{C}^{p} \right)^{-1} \right]^{-1} : D(\Delta\boldsymbol{\varepsilon}) \,, \tag{36}$$

with $\mathbf{C}^{p} = \mathbf{h}_X \boldsymbol{\xi} + h_\tau \boldsymbol{\xi} \otimes \boldsymbol{\xi} + \tau_{n+1} \boldsymbol{\zeta}$ being the tangent operator linearly relating the deviatoric stress increment to the plastic strain increment, $D\boldsymbol{\sigma}'_{n+1} = \mathbf{C}^{p} : D(\Delta\boldsymbol{\varepsilon}^{p})$.

Calculation of the algorithmic modulus with Eq. (36) involves two matrix inversions. This numerical inconveniency can be avoided if the tangent modulus is derived in a slightly different manner, starting from Eq. (25). By differentiation of Eq. (25) and convenient rearrangement of terms, one obtains:

$$\underbrace{\left[\frac{\partial \mathbf{X}_{n+1}}{\partial(\Delta\boldsymbol{\varepsilon}^{p})} + \boldsymbol{\xi} \otimes \frac{\partial \tau_{n+1}}{\partial(\Delta\boldsymbol{\varepsilon}^{p})} + \tau_{n+1}\boldsymbol{\zeta} + \mathbf{C}^{e} : \mathbf{I}_4^{\prime s} \right]}_{\mathcal{K}} : D(\Delta\boldsymbol{\varepsilon}^{p}) = \mathbf{C}^{e} : D(\Delta\boldsymbol{\varepsilon}') \,. \tag{37}$$

Therefore, the following relationship can be written:

$$D\Delta\boldsymbol{\varepsilon}^{p} = \mathcal{K}^{-1} : \mathbf{C}^{e} : D\Delta\boldsymbol{\varepsilon}' \tag{38}$$

where $\mathcal{K}$ is a matrix related to $\mathbf{C}^{p}$, yet different. The major advantage of this formula is that $\mathcal{K} \equiv \partial\boldsymbol{\rho}(\Delta\boldsymbol{\varepsilon}^{p}) / \partial(\Delta\boldsymbol{\varepsilon}^{p})$, as one can easily see from Eq. (27). Consequently, $\mathcal{K}$ and its inverse have already been computed during the calculation for $\Delta\boldsymbol{\varepsilon}^{p}$.

Finally, the incremental form of Hooke's law is differentiated in its split form (20)-(21) and then combined using Eq. (38) to obtain:

$$D\boldsymbol{\sigma}_{n+1} = \mathbf{C}^{alg} : D\Delta\boldsymbol{\varepsilon} \quad \text{with} \qquad \mathbf{C}^{alg} = \mathbf{C}^{e} - \mathbf{C}^{e} : \mathcal{K}^{-1} : \mathbf{C}^{e} \,. \tag{39}$$

An interesting characteristic of this new formulation, in addition to its simplicity, is that no extra matrix inversions are needed, except for the Jacobian of Eq. (25), which is already available in triangular form. Note that in the case of isotropic linear elasticity, the algorithmic tangent modulus further simplifies as

$$\mathbf{C}^{alg} = K\mathbf{I}\otimes\mathbf{I} + 2G\mathbf{I}_4'^{s} - 4G^2\mathcal{K}^{-1}. \tag{40}$$

3.4 Sub-stepping procedure

In order to ensure a quadratic convergence of the Newton-Raphson resolution of Eq. (25), a consistent tangent modulus has been derived from the discrete equations. However, the solution of the nonlinear Eq. (25) can fail to converge for large strain increments, especially when the plastic potential exhibits strong variations of curvature. For example, this appeared to be the case for the Yld2004-18p yield criterion [40], when small values of the exponent *b* are considered, as shown by Yoon et al. [41]. The strain-rate potential Srp2004-18p, proposed by Barlat and Chung [42] and Kim *et al.* [9], has also shown such difficulties when the validations that will be shown in Section 4 were performed. Similar numerical difficulties have been reported in the literature, when using highly flexible anisotropic yield criteria. A sub-stepping procedure has been adopted to solve this problem, inspired from previous yield-surface based works performed in the classical plasticity framework [43-47]. When the initial solution $\Delta\boldsymbol{\varepsilon}^p_{(0)}$ induces a too large value of the residual, which prevents convergence, this value is used to generate a user-defined number *m* of constant vectors, with the following rule:

$$\bar{\boldsymbol{\rho}}_i = \frac{m-i}{m}\boldsymbol{\rho}\left(\Delta\boldsymbol{\varepsilon}^p_{(0)}\right), \quad i=\overline{1,m}. \tag{41}$$

Then, the following series of equations are solved sequentially, using the solution $\Delta\boldsymbol{\varepsilon}^p_{(i)}$ of equation "*i*" as an initial guess for equation "*i*+1":

$$\boldsymbol{\rho}\left(\Delta\boldsymbol{\varepsilon}^p_{(i)}\right) - \bar{\boldsymbol{\rho}}_i = 0, \quad i=\overline{1,m}. \tag{42}$$

At the end of this procedure, the solution of the initial equation is obtained, since according to Eq. (41), $\bar{\boldsymbol{\rho}}_m = \mathbf{0}$. Note that this sub-stepping procedure is activated only at the time steps and integration points where the direct solution of Eq. (25) fails. Consequently, the impact on the overall computation time is reduced. The user-defined number of sub-steps *m* can be increased automatically by the code in case of divergence.

The initialization of the plastic strain rate increment has an important impact on the convergence. In particular, the initial value for the plastic strain increment cannot be zero, since it enters the very definition of the plastic potential. The most satisfactory initialization was

found to be $\Delta\boldsymbol{\varepsilon}^{p}_{(0)} = \Delta\lambda_{(0)}\mathbf{N}_{(0)}$, where $\mathbf{N}_{(0)}$ is the direction normal to a von Mises yield surface passing through the elastic trial stress.

Note that, just for avoiding similar cases where the nonlinearity of the plastic potential would prevent the convergence of the minimization problem (31), a similar sub-stepping algorithm has been implemented that allows for a robust solution of both equations.

3.5 Overall time integration algorithm

The numerical implementation has been performed in Abaqus/Standard via a UMAT routine. For clarity, the numerical algorithm is summarized hereafter. It has been used in the next section for several validations and applications, in order to address its robustness and usefulness.

1. Input data: $\boldsymbol{\sigma}_n,\ \mathbf{X}_n,\ \tau_n,\ \Delta\boldsymbol{\varepsilon}$ *(strain increment, initial stress and internal variables)*
2. Compute $\sigma^{sph}_n, \Delta\varepsilon^{sph}, \boldsymbol{\sigma}'_n, \Delta\boldsymbol{\varepsilon}'$ *(spherical and deviatoric parts)*
3. Elastic prediction: $\boldsymbol{\sigma}'^{try} = \boldsymbol{\sigma}'_n + \mathbf{C}^{e} : \Delta\boldsymbol{\varepsilon}'$
4. Plastic yield condition: $\mathrm{sgn}\left\{\min_{\mathbf{N}}\left[\tau_n\Psi(\mathbf{N}) - \left(\boldsymbol{\sigma}'^{try} - \mathbf{X}_n\right) : \mathbf{N}\right]\right\}$?
5. If elastic increment:
   $\boldsymbol{\sigma}_{n+1} = \boldsymbol{\sigma}'^{try} + \boldsymbol{\sigma}^{sph}_n + Ktr(\Delta\boldsymbol{\varepsilon})\mathbf{I}$
   $\mathbf{X}_{n+1} = \mathbf{X}_n, \quad \tau_{n+1} = \tau_n$
   $\mathbf{C}^{alg} = \mathbf{C}^{e}$
6. Otherwise (elastoplastic increment):
   Initialize $\Delta\boldsymbol{\varepsilon}^{p}$
   Repeat:
   Calculate $\Delta\lambda,\ \boldsymbol{\xi}(\Delta\boldsymbol{\varepsilon}^{p}),\ \boldsymbol{\zeta}(\Delta\boldsymbol{\varepsilon}^{p})$ *(specific to chosen potential)*
   Calculate $\mathbf{X}_{n+1},\ \tau_{n+1},\ \dfrac{\partial\mathbf{X}_{n+1}}{\partial(\Delta\boldsymbol{\varepsilon}^{p})},\ \dfrac{\partial\tau_{n+1}}{\partial(\Delta\boldsymbol{\varepsilon}^{p})}$ *(specific to hardening model)*
   Calculate $\boldsymbol{\rho}(\Delta\boldsymbol{\varepsilon}^{p}),\ \dfrac{\partial\boldsymbol{\rho}(\Delta\boldsymbol{\varepsilon}^{p})}{\partial(\Delta\boldsymbol{\varepsilon}^{p})}$; update $\Delta\boldsymbol{\varepsilon}^{p}$ *(BFGS algorithm)*
   Until convergence
   Update stress and state variables; calculate the consistent tangent modulus $\mathbf{C}^{alg}$
7. Return $\boldsymbol{\sigma}_{n+1}$, state variables, and $\mathbf{C}^{alg}$ to check equilibrium.

4 ALGORITHM VALIDATION AND APPLICATIONS

The constitutive algorithm developed in Section 3 has been implemented in the finite element code Abaqus/Standard and applied to typical sheet metal forming problems. One aim of this

section is to validate the state update algorithm with respect to equivalent models available in Abaqus. Secondly, an advanced anisotropic strain-rate potential is implemented in the same framework and its predictions are compared to a yield function similar in form and shown to behave as its quasi-dual [9].

4.1 Plastic potentials and hardening model

The constitutive model presented in Section 2 must be completed by the mathematical expressions of the plastic potential $\Psi(\mathbf{D}^p)$ and of the internal variables τ and $\mathbf{X}$. Two examples of plastic potentials are considered hereafter. One is the quadratic strain-rate potential dual to the classical Hill yield criterion, mainly used for validation purposes. Next, the anisotropic strain-rate potential Srp2004-18p [9, 42] has been implemented. As for the hardening, a non-linear isotropic-kinematic model is implemented, which is also available in Abaqus. Indeed, hardening is not an issue in this work – validation is the main issue here –, and more complex hardening models can be adopted within the present framework.

Quadratic plastic potential

The yield criterion proposed in 1948 by Hill [48] is a quadratic expression with six material parameters (*F*, *G*, *H*, *L*, *M,* and *N*). In the material orthotropic frame, this criterion can be written as:

$$\Phi(\boldsymbol{\sigma},\mathbf{X},\tau)=\left[F\left(T_{22}-T_{33}\right)^2+G\left(T_{33}-T_{11}\right)^2+H\left(T_{11}-T_{22}\right)^2+2LT_{23}^2+2MT_{31}^2+2NT_{12}^2\right]^{\frac{1}{2}}-\tau \quad (43)$$

where the three axes 1, 2, and 3 are the rolling, transverse and normal direction, respectively, in the case of a rolled, orthotropic metal sheet, and T_{ij} are the components of the effective stress tensor. Its dual strain-rate potential can be rigorously derived [14] and takes the form:

$$\Psi\left(\mathbf{D}^p\right)=\left[\frac{4F}{\Delta}\left(D_{11}^p\right)^2+\frac{4G}{\Delta}\left(D_{22}^p\right)^2+\frac{4H}{\Delta}\left(D_{33}^p\right)^2+\frac{2}{L}\left(D_{23}^p\right)^2+\frac{2}{M}\left(D_{31}^p\right)^2+\frac{2}{N}\left(D_{12}^p\right)^2\right]^{\frac{1}{2}} \quad (44)$$

where $\Delta=FH+FG+HG$. For an isotropic material, $F=G=H=1/2$ and $L=M=N=3/2$.

Srp2004-18p plastic potential

An extension of the Srp93 strain-rate potential [6] has been recently proposed by Barlat and Chung [42] and Kim *et al.* [9]. This potential, named Srp2004-18p, has consistently proven to have superior flexibility and ability to describe the anisotropy of sheet metal for a large range of materials [24, 49]. Its mathematical expression involves 18 material parameters and makes use of two linear transformations of the plastic strain-rate tensor $\mathbf{D}^p$:

$$\Psi\left(\mathbf{D}^p\right)=\left[\frac{1}{2^{2-b}+2}\left(\left|\tilde{E}_1'\right|^b+\left|\tilde{E}_2'\right|^b+\left|\tilde{E}_3'\right|^b+\left|\tilde{E}_2''+\tilde{E}_3''\right|^b+\left|\tilde{E}_3''+\tilde{E}_1''\right|^b+\left|\tilde{E}_1''+\tilde{E}_2''\right|^b\right)\right]^{\frac{1}{b}}, \quad (45)$$

where $\tilde{E}_i'$ and $\tilde{E}_i''$, $i=\overline{1,3}$ are the principal values of $\tilde{\mathbf{D}}^{p'}$ and $\tilde{\mathbf{D}}^{p''}$, defined respectively by the two linear transformations hereafter:

$$\tilde{\mathbf{D}}^{p'}=\mathbf{A}'\cdot\mathbf{I}_4'^s\cdot\mathbf{D}^p, \quad (46)$$

$$\tilde{\mathbf{D}}^{p''}=\mathbf{A}''\cdot\mathbf{I}_4'^s\cdot\mathbf{D}^p. \quad (47)$$

The fourth order arrays $\mathbf{A}'$ and $\mathbf{A}''$ contain anisotropy coefficients. For the case of orthotropic symmetry, they can be represented as the following 6×6 arrays:

$$\mathbf{A}'=\begin{bmatrix}0 & -a_1 & -a_2 & 0 & 0 & 0\\ -a_3 & 0 & -a_4 & 0 & 0 & 0\\ -a_5 & -a_6 & 0 & 0 & 0 & 0\\ 0 & 0 & 0 & a_7 & 0 & 0\\ 0 & 0 & 0 & 0 & a_8 & 0\\ 0 & 0 & 0 & 0 & 0 & a_9\end{bmatrix} \text{ and } \mathbf{A}''=\begin{bmatrix}0 & -a_{10} & -a_{11} & 0 & 0 & 0\\ -a_{12} & 0 & -a_{13} & 0 & 0 & 0\\ -a_{14} & -a_{15} & 0 & 0 & 0 & 0\\ 0 & 0 & 0 & a_{16} & 0 & 0\\ 0 & 0 & 0 & 0 & a_{17} & 0\\ 0 & 0 & 0 & 0 & 0 & a_{18}\end{bmatrix} \quad (48)$$

In order to use these compact notations, the $\mathbf{D}^p$-like tensors are written as 6-component vectors; i.e., $\mathbf{D}^p=[D_{11}^p \quad D_{22}^p \quad D_{33}^p \quad D_{23}^p \quad D_{31}^p \quad D_{12}^p]^T$, with components in the frame of material symmetry.

The isotropic case is obtained for $a_1=a_2=...=a_{18}=1$ and b = 4/3 or 3/2 for bcc or fcc materials, respectively. The Srp93 potential can be recovered by enforcing

$$\mathbf{A}'\cdot\mathbf{I}_4'^s=\mathbf{A}''\cdot\mathbf{I}_4'^s=\mathbf{A}. \quad (49)$$

Recently, an extension of Srp93 and Srp2004-18p has been proposed by Rabahallah et al. [50], involving an arbitrary number of linear transformations.

The first-order derivatives of the expression (45) are provided in [9]. The implicit time integration procedure also requires the calculation of the second order derivatives.

Hardening model

Modelling of hardening has been a very active research field in the last decades, especially for sheet metal forming applications, due to an increased interest in the accurate description of strain-path changes in finite element simulations (e.g., strain reversal, orthogonal loading etc.;

an overview can be found in Haddadi *et al*. [51]). Several advanced hardening models have been proposed in the last two decades [36, 52-55]. In order to be implemented directly in the present algorithm, the hardening model must take the form (10). This may seem a restrictive condition; however, it has been demonstrated that even hardening models as complex as the Teodosiu-Hu model [36, 51, 56, 57] can be cast in such a simple form, without any alteration [19, 38, 58, 59].

For the sake of comparison, the non-linear isotropic-kinematic hardening model implemented in the current algorithm is the one already available in Abaqus/Standard [60]. This model involves two internal variables (R, $\mathbf{X}$). The scalar variable R describes the isotropic hardening, and the second-order tensor $\mathbf{X}$ describes the kinematic hardening. With the notation of Section 2, the differential equations and the initial conditions describing the evolution of the hardening variables are:

$$\tau = \tau_0 + R\,, \tag{50}$$

$$\dot{R} = C_{\mathrm{R}}\left(R_{\mathrm{sat}} - R\right)\dot{\lambda}, \qquad R(0) = 0\,, \tag{51}$$

$$\dot{\mathbf{X}} = C_{\mathrm{x}}\left(X_{\mathrm{sat}}\boldsymbol{\xi} - \mathbf{X}\right)\dot{\lambda}, \qquad \mathbf{X}(0) = \mathbf{0}\,, \tag{52}$$

where $\tau_0, C_{\mathrm{R}}, R_{\mathrm{sat}}, C_{\mathrm{x}}$ and X_{sat} are material parameters.

The backward Euler scheme is used for the time integration of these rate equations, leading to the update equations:

$$\begin{aligned} \tau_{n+1} &= \tau_0 + \frac{R_n + C_R R_{sat}\Delta\lambda}{1 + C_R\Delta\lambda}, \\ \mathbf{X}_{n+1} &= \frac{\mathbf{X}_n + C_x X_{sat}\boldsymbol{\xi}_{n+1}\Delta\lambda}{1 + C_x\Delta\lambda}. \end{aligned} \tag{53}$$

The following derivatives are also required for the calculation of the algorithmic tangent modulus:

$$\begin{aligned} \frac{\partial \mathbf{X}_{n+1}}{\partial(\Delta\boldsymbol{\varepsilon}^p)} &= \frac{C_x X_{sat}\boldsymbol{\zeta}\left(C_x\Delta\lambda^2 + \Delta\lambda\right) + C_x X_{sat}\boldsymbol{\xi}\otimes\boldsymbol{\xi} - C_x\mathbf{X}_n\otimes\boldsymbol{\xi}}{\left(1 + C_x\Delta\lambda\right)^2} \\ \frac{\partial \tau_{n+1}}{\partial(\Delta\boldsymbol{\varepsilon}^p)} &= \frac{\left(C_R R_{sat} - R_n C_R\right)\boldsymbol{\xi}}{\left(1 + C_R\Delta\lambda\right)^2} \end{aligned} \tag{54}$$

These particular expressions of the plastic potential and hardening laws, as well as their derivatives, simply feed into the general algorithm without any other modification. Any other model that fits the requirements of Section 2 can be implemented with this algorithm in the same way.

4.2 Algorithm validation: bulge test and S-shape rail forming

These applications are meant to validate the numerical implementation of the constitutive algorithm with respect to reference results, and to address its computational efficiency with respect to the more classical yield-function-based algorithms. To do so, two typical sheet metal forming tests have been selected: a bulge test and an S-shape rail forming. The main difference between the two is the highly nonlinear contact evolution for the S-rail, which may cause convergence problems that further interact with the overall equilibrium convergence sequence. In both cases, Hill's quadratic potential is used. Since the quadratic Hill yield criterion implemented in Abaqus/Standard is the exact dual of the quadratic potential used here, an identical response should be expected.

The material parameters, corresponding to an 1-mm thick AA5182 aluminium sheet, are given in Table 1 (from Haddadi *et al*. [51]). The incompatible-modes enriched, hybrid displacement-pressure element C3D8IH is used throughout this section.

Table 1. Material parameters used for the numerical simulations.

Elasticity		*Hill'48 anisotropy*						**Hardening**				
E	ν	F	G	H	L	M	N	τ_0	C_R	R_{sat}	C_X	X_{sat}
[MPa]								[MPa]		[MPa]		[MPa]
70000	0.33	0.65	0.57	0.43	1.5	1.5	1.61	148.5	9.7	192.4	152.7	26

The results for the bulge test simulations and the S-rail simulations are shown in Figures 2 and 3, respectively. The two figures clearly show that the results obtained with the Abaqus built-in model and algorithm, and with the current implementation via UMAT, do coincide with each other. This perfect correspondence has been also noticed in terms of individual components of stress, strain, and internal variables. Thus the numerical implementation of the constitutive algorithm seems accurate and error-free, at least in such typical applications.

Table 2 summarizes the computing time required by two simulations, using the Abaqus built-in Hill quadratic criterion, as well as its dual potential via UMAT. The calculations have been run on a PC computer with a Pentium 1.8 GHz dual core processor. The two dual quadratic potentials (and the corresponding computer implementations) give not only identical predictions, but the computing time is almost the same (less than 5% larger in the strain-rate potential case).

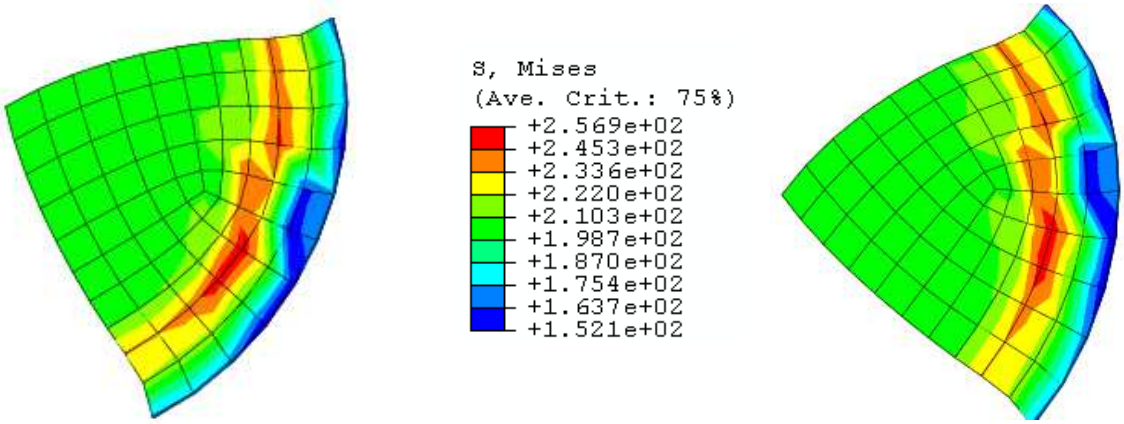

Figure 2. Finite element simulation results for the bulge test. Left: using the Abaqus/Standard built-in model and algorithm; Right: using the current model and algorithm implemented in Abaqus/Standard via UMAT. Isovalues of equivalent stress.

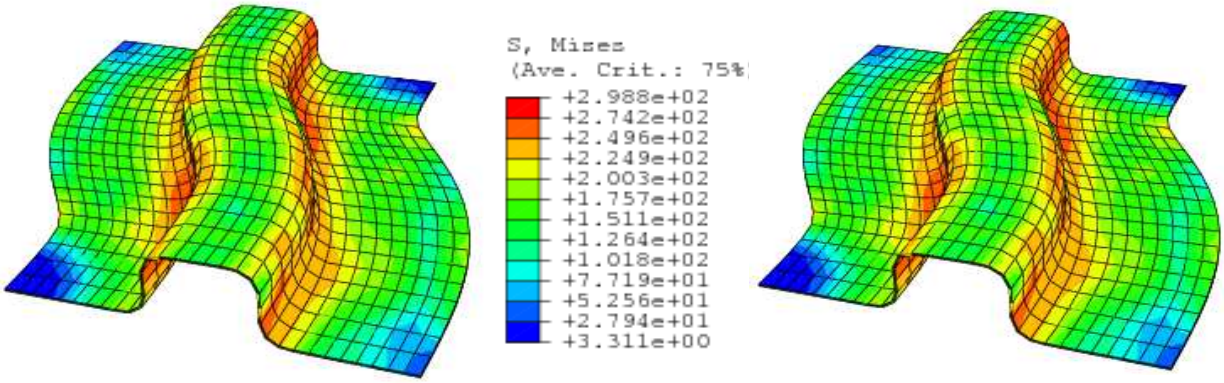

Figure 3. Finite element simulation results for the S-rail. Left: using the Abaqus/Standard built-in model and algorithm; Right: using the current model and algorithm implemented in Abaqus/Standard via UMAT. Isovalues of equivalent stress.

Table 2. CPU time and number of increments for the numerical simulations of bulge test and S-shape rail.

Forming problem	*Code*	*CPU time*	***Number of increments***
Bulge test	Abaqus	32 min	73
	UMAT	33 min	73
S-shape rail	Abaqus	211 min	240
	UMAT	219 min	240

4.3 Cup drawing simulation with Srp2004-18p

The aim of this application is twofold. First, the currently developed algorithm is applied to one of the most complex strain-rate potentials available in the literature, in order to address its robustness. Second, its finite element predictions are compared to those of its "pseudo-conjugate" yield function, Yld2004-18p, for a first investigation of their relative equivalence. The Yld2004-18p criterion has been used for the cup drawing simulation of an AA2090 aluminium alloy by Yoon *et al.* [41]. Kim *et al.* [23] have recently used plane-stress versions of both Yld2004-18p and Srp2004-18p for this application. The parameters of several strain-rate potentials, including Srp2004-18p, have been identified for the same material by Rabahallah et al. [24]. Therefore, the same cup drawing simulation was performed with the algorithms developed in this paper, using the anisotropy coefficients of the AA2090 material. The hardening parameters are those used in [41]. Table 3 summarizes the material parameters used in the simulation. The geometry of the test is given in Figure 4. The sheet thickness was 1.6 mm, and the blank holder force was 5500 N. The Coulomb friction coefficient between the sheet and the tools was 0.1. One layer of linear hybrid (displacement-pressure) C3D8IH solid elements has been used to mesh one quarter of the sheet metal, as parametric numerical studies have shown that the number of solid element layers does not influence the earring profile [59, 61].

Table 3. Material parameters used for the cup drawing simulation.

(a) Elasticity and hardening parameters

Elasticity		**Hardening**				
E [MPa]	ν	τ_0 [MPa]	C_R	R_{sat} [MPa]	C_X	X_{sat} [MPa]
70000	0.3	279.6	1.7	488	0	0

(b) Anisotropy parameters

a_1	a_2	a_3	a_4	a_5	a_6	a_7	a_8	a_9
0.39	0.68	0.91	1.01	1.13	0.63	1.00	0.56	1.07
a_{10}	a_{11}	a_{12}	a_{13}	a_{14}	a_{15}	a_{16}	a_{17}	a_{18}
1.37	0.77	1.45	0.68	0.94	1.11	1.00	0.56	0.51
b=1.3333								

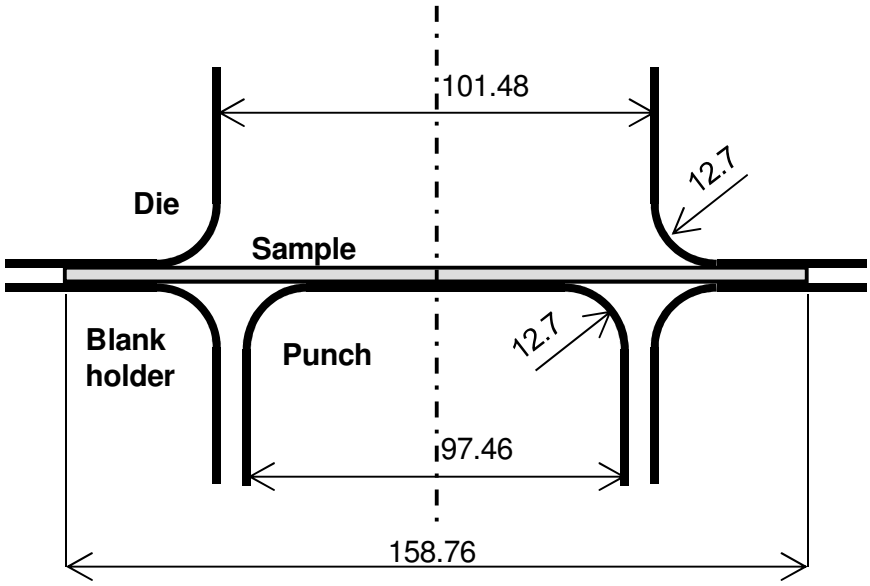

Figure 4. Test geometry for the cup drawing simulation. Dimensions are in mm.

Figure 5 shows the results in terms of cup height profiles. The results obtained with the current implementation are compared to those available in [41] and [23]. One may notice that, although the four predictions are slightly different, they present similar characteristics: six ears are predicted, at the same location, and the errors with respect to the experiments are of the same order and similarly distributed. It is noteworthy that very few other stress or strain-rate potentials allow for the prediction of six ears in cup drawing. Thus, this simulation underlines the mathematical flexibility of the Srp2008-18p potential and its ability to describe complex anisotropic behaviour within a phenomenological framework. Both Srp2004-18p predictions underestimate the ears at 0° and 180°, as compared to Yld2004-18p. Also, the differences between three-dimensional and plane stress formulations are as large as those between the stress and strain-rate potentials, respectively. A more detailed interpretation of the differences existing between the four predictions is difficult for several reasons. The parameter identification method used for our model is different from the three other. Also, two different finite element codes have been used (namely, MSC.Marc for the 3D Yld2004-18p model and Abaqus for the other models), with different elements. Thus, the comparison in Figure 5 cannot be refined any further, unless all the simulations are performed with the same finite element code, mesh, and parameters identified in the same manner. Such a comparison would allow a more detailed investigation of the "quasi-duality" of the two functions from a practical point of view. The recent results in [23] suggest that the predictions of the in-plane variation of tensile yield stress and anisotropy coefficient may be slightly different between Yld2004-18p and Srp2004-18p, thus explaining part of the variability in Figure 5.

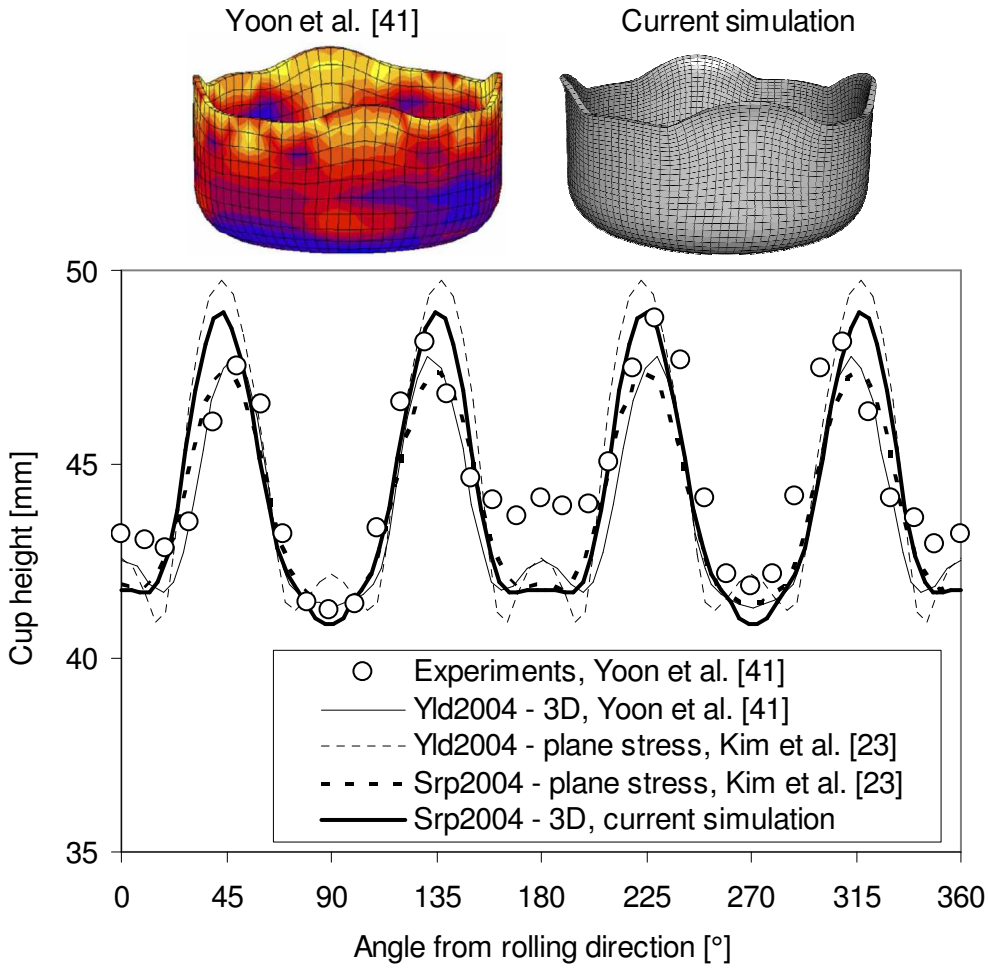

Figure 5. Results of the numerical simulation of cup drawing with Srp2004-18p; cup height profiles for the current simulation and the reference simulations in [41] and [23], compared to experiments.

5 CONCLUSIONS

A fully implicit state update algorithm for strain-rate-potential-based time-independent, anisotropic, large strain elastoplasticity models has been developed and described in detail. This paper provides a generic framework for the numerical implementation of various models that fall into this category. The numerical implementation of this algorithm in the commercial FE code Abaqus/Standard is accurate and robust enough to simulate typical sheet forming operations.

The minimization problem that overcomes the absence of an explicit yield condition has been shown to induce virtually no additional cost. Therefore, yield-function-based and strain-rate-potential-based constitutive algorithms can be considered equivalent in terms of numerical efficiency. The recent Srp2004-18p has been implemented in this framework and has shown predictive capabilities similar to the Yld2004-18p yield criterion, especially the ability to predict six-ear cup drawing profiles.

ACKNOWLEDGEMENTS

The authors are grateful to Frédéric Barlat for providing material data and simulation results, and to Kwansoo Chung and Brigitte Bacroix for fruitful discussions. The three-year financial support from the Région Lorraine and from the Centre National de la Recherche Scientifique (CNRS) for the first author is gratefully acknowledged.

APPENDIX – COMPACT NOTATION FOR DEVIATORIC AND UNIT-LENGTH TENSORS

Most tensor quantities involved in the plasticity equations (e.g., **N**) are symmetric and deviatoric, hence a five-component notation can be adopted to reduce the number of independent unknowns in the calculations:

$$\begin{aligned} N_1 &= \frac{1}{\sqrt{2}}\left(N_{11} - N_{22}\right) \\ N_2 &= \sqrt{\frac{3}{2}}\left(N_{11} + N_{22}\right) \\ N_3 &= \sqrt{2}N_{23} \\ N_4 &= \sqrt{2}N_{31} \\ N_5 &= \sqrt{2}N_{12} \end{aligned} \tag{55}$$

Moreover, the minimization in Eq. (30) is performed with respect to the unit-length deviatoric symmetric tensor **N** which has only four independent components. In order to reduce the size of the problem and to avoid minimization under constraints, four angles are used to define **N**, as follows:

$$
\begin{aligned}
N_1 &= \cos\theta_1 \sin\theta_2 \sin\theta_3 \sin\theta_4 \\
N_2 &= \sin\theta_1 \sin\theta_2 \sin\theta_3 \sin\theta_4 \\
N_3 &= \cos\theta_2 \sin\theta_3 \sin\theta_4 \\
N_4 &= \cos\theta_3 \sin\theta_4 \\
N_5 &= \cos\theta_4
\end{aligned}
\tag{56}
$$

where $0 \leq \theta_1 \leq 2\pi$ and $0 \leq \theta_i \leq \pi$, for i between 2 and 4.

This contracted notation has several useful properties. Thus, it is easy to verify that the scalar products of two tensors **A** and **B** verify the following equalities

$$
\mathbf{A} : \mathbf{B} = A_{ij} B_{ij} = A_I B_I \quad ; \quad I = \overline{1,5} \; ; \; i \text{ and } j = \overline{1,3} \tag{57}
$$

and, as a consequence, the norm of the tensor **A** verifies

$$
\|\mathbf{A}\| = \sqrt{A_{ij} A_{ij}} = \sqrt{A_I A_I} \; . \tag{58}
$$

REFERENCES

1. Ziegler H. *An introduction to thermomechanics*. North-Holland: Amsterdam, 1977.

2. Hill R. Constitutive dual potentials in classical plasticity. *Journal of Mechanics and Physics of Solids* 1987; **35**:22-33.

3. Arminjon M, Bacroix B. On plastic potentials for anisotropic metals and their derivation from the texture function. *Acta Mechanica* 1991; **88**(3-4):219-243.

4. Arminjon M, Bacroix B, Imbault D, Raphanel JL. A fourth-order plastic potential for anisotropic metals and its analytical calculation from the texture function. *Acta Mechanica* 1994; **107**(1-4):33-51.

5. Van Houtte P, Mols K, Van Bael A, Aernoudt E. Application of yield loci calculated from texture data. *Textures Microstruct* 1989; **11**:23-39.

6. Barlat F, Chung K. Anisotropic potentials for plastically deforming metals. *Modelling and Simulation in Materials Science and Engineering* 1993; **1**(4):403-416.

7. Barlat F, Chung K, Richmond O. Strain rate potential for metals and its application to minimum plastic work path calculations. *International Journal of Plasticity* 1993; **9**(1):51-63.

8. Chung K, Barlat F, Richmond O, Yoon JW. Blank design for a sheet forming application using the anisotropic strain-rate potential Srp98. in Zabaras et al. (ed.), *The integration of Material, Process and Product Design*. Balkema: Rotterdam, 1999, 213-219.

9. Kim D, Barlat F, Bouvier S, Rabahallah M, Balan T, Chung K. Non-quadratic anisotropic potentials based on linear transformation of plastic strain rate. *International Journal of Plasticity* 2007; **23**(8):1380-1399.

10. Yoon JW, Song IS, Yang DY, Chung K, Barlat F. Finite element method for sheet forming based on an anisotropic strain-rate potential and the convected coordinate system. *International Journal of Mechanical Sciences* 1995; **37**:733-752.

11. Chung K, Barlat F, Brem JC, Lege DJ, Richmond O. Blank shape design for a planar anisotropic sheet based on ideal forming design theory and fem analysis. *International Journal of Mechanical Sciences* 1997; **39**(1):105-120.

12. Chung K, Lee SY, Barlat F, Keum YT, Park JM. Finite element simulation of sheet forming based on a planar anisotropic strain-rate potential. *International Journal of Plasticity* 1996; **12**(1):93-115.

13. Richmond O, Chung K. Ideal stretch forming for minimum weight axisymmetric shell structures. *International Journal of Mechanical Sciences* 2000; **42**(12):2455-2468.

14. Bacroix B, Gilormini P. Finite-element simulations of earing in polycrystalline materials using a texture-adjusted strain-rate potential. *Modelling and Simulation in Materials Science and Engineering* 1995; **3**(1):1-21.

15. Szabo L, Jonas JJ. Consistent tangent operator for plasticity models based on the plastic strain rate potential. *Computer Methods in Applied Mechanics and Engineering* 1995; **128**:315-323.

16. Van Houtte P, Van Bael A, Winters J. The incorporation of texture-based yield loci into elasto-plastic finite element programs. *Textures and Microstructures* 1995; **24**:255-272.

17. Hoferlin E, Li S, Van Bael A, Van Houtte P. Texture- and microstructure- induced anisotropy: micro-macro modeling, implementation. in Mori K. (ed.), *Simulation of Materials Processing: Theory, Methods and Applications, Proc of Int Conf Numiform 2001*. Swets & Zeiltinger, 2001, 209-214.

18. Li S, Hoferlin E, Van Bael A, Van Houtte P. Application of a texture-based plastic potential in earing prediction of an IF steel. *Advanced Engineering Materials* 2001; **3**(12):990-994.

19. Li S, Hoferlin E, Van Bael A, Van Houtte P, Teodosiu C. Finite element modeling of plastic anisotropy induced by texture and strain-path change. *International Journal of Plasticity* 2003; **19**(5):647-674.

20. Zhou Y, Jonas JJ, Savoie J, Makinde A, MacEwen SR. Effect of texture on earing in FCC metals: Finite element simulations. *International Journal of Plasticity* 1998; **14**(1-3):117-138.

21. Zhou Y, Jonas JJ, Szabo L, Makinde A, Jain M, MacEwen SR. Incorporation of an anisotropic (texture-based) strain-rate potential into three-dimensional finite element simulations. *International Journal of Plasticity* 1997; **13**(1-2):165-181.

22. Savoie J, MacEwen SR. A sixth order inverse function for incorporation of crystallographic texture into predictions of properties of aluminium sheet. *Textures and Microstructures* 1996; **26/27**:495-512.

23. Kim JH, Lee MG, Barlat F, Wagoner RH, Chung K. An elasto-plastic constitutive model with plastic strain rate potentials for anisotropic cubic metals. *International Journal of Plasticity* 2008; **24**(12):2298-2334.

24. Rabahallah M, Balan T, Bouvier S, Bacroix B, Barlat F, Chung K, Teodosiu C. Parameter identification of advanced plastic potentials and impact on plastic anisotropy prediction. *International Journal of Plasticity* 2009; **25**(3):491-512.

25. Mandel J. Définition d'un repère privilégié pour l'étude des transformations anélastiques du polycristal. *Journal de Mécanique Théorique et Appliquée* 1982; **1**:7-23.

26. Kuroda M. Interpretation of the behavior of metals under large plastic shear deformations: a macroscopic approach. *International Journal of Plasticity* 1997; **13**(4):359-383.

27. Peeters B, Hoferlin E, Van Houtte P, Aernoudt E. Assessment of crystal plasticity based calculation of the lattice spin of polycrystalline metals for FE implementation. *International Journal of Plasticity* 2001; **17**:819-836.

28. Dafalias YF. Plastic spin: necessity or redundancy. *International Journal of Plasticity* 1998; **14**:909-931.

29. Han CS, Choi Y, Lee JK, Wagoner RH. A FE formulation for elasto-plastic materials with planar anisotropic yield functions and plastic spin. *International Journal of Solids and Structures* 2002; **39**(20):5123-5141.

30. Duchêne L, Lelotte T, Flores P, Bouvier S, Habraken AM. Rotation of axes for anisotropic metal in FEM simulations. *International Journal of Plasticity* 2008; **24**(3):397-427.

31. Hiwatashi S, Van Bael A, Van Houtte P, Teodosiu C. Modelling of plastic anisotropy based on texture and dislocation structure. *Computational Materials Science* 1997; **9**(1-2):274-284.

32. Hughes TJR. Numerical implementation of constitutive models: rate-independent deviatoric plasticity. in Nemat-Nasser S., Asaro R.J., Hegemier G.A. (eds.), *Theoretical foundation for large-scale computations for nonlinear material behavior*. Martinus Nij Publishers: Dordrecht, The Netherlands, 1984, 29-57.

33. Simo J, Taylor R. Consistent tangent operators for rate-independent elasto-plasticity. *Computer Methods in Applied Mechanics and Engineering* 1985; **48**:101-118.

34. Ortiz M, Popov EP. Accuracy and stability of integration algorithms for elastoplastic constitutive relations. *International Journal for Numerical Methods in Engeneering* 1985; **21**:1561-1576.

35. Balan T, Teodosiu C. Constitutive algorithm for plasticity model of texture, strain-path induced anisotropy and rate-sensitivity: Interface between constitutive algorithm and FE code (Abaqus/ Standard), Internal report. University Paris 13, 1999.

36. Teodosiu C, Hu Z. Microstructure in the continuum modeling of plastic anisotropy. *19th Riso International Symposium on Materials Science Proceedings*, Roskilde, 1998; 149-168.

37. Bacroix B, Gilormini P. Unpublished work. 1994;

38. Hoferlin E. Incorporation of an accurate model of texture and strain-path induced anisotropy in simulations of sheet metal forming. Katholieke Universiteit Leuven, 2001

39. Bird WW, Martin JB. Consistent predictors and the solution of the piecewise holonomic incremental problem in elasto-plasticity. *Engineering Structures* 1990; **12**:9-14.

40. Barlat F, Aretz H, Yoon JW, Karabin ME, Brem JC, Dick RE. Linear transfomation-based anisotropic yield functions. *International Journal of Plasticity* 2005; **21**(5):1009-1039.

41. Yoon JW, Barlat F, Dick RE, Karabin ME. Prediction of six or eight ears in a drawn cup based on a new anisotropic yield function. *International Journal of Plasticity* 2006; **22**(1):174-193.

42. Barlat F, Chung K. Anisotropic strain rate potential for aluminum alloy plasticity. in Banabic D. (ed.), *8th ESAFORM Conference*. The Publishing House of the Romanian Academy: Cluj-Napoca, Romania, 2005, 415-418.

43. Yoon JW, Yang DY, Chung K. Elasto-plastic finite element method based on incremental deformation theory and continuum based shell elements for planar anisotropic sheet materials. *Computer Methods in Applied Mechanics and Engineering* 1999; **174**:23-56.

44. Yoon JW, Yang DY, Chung K, Barlat F. General elasto-plastic finite element formulation based on incremental deformation theory for planar anisotropy and its application to sheet metal forming. *International Journal of Plasticity* 1999; **15**(1):35-67.

45. Ortiz M, Simo JC. An analysis of a new class of integration algorithms for elastoplastic relations. *International Journal for Numerical Methods in Engeneering* 1986; **23**:353-366.

46. Park MS, Lee BC. Geometrically nonlinear and elastoplastic three dimensional shear flexible beam element of Von-Mises type hardening material. *International Journal for Numerical Methods in Engeneering* 1996; **39**:383-408.

47. Dutko M, Peric D, Owen DRJ. Universal anisotropic yield criterion based on superquadratic functional representation: Part 1. Algorithmic issues and accuracy analysis. *Computer Methods in Applied Mechanics and Engineering* 1993; **109**:73-93.

48. Hill R. A theory of the yielding and plastic flow of anisotropic metals. *Proc Roy Soc A* 1948; **193**:281-297.

49. Rabahallah M. Modélisation de l'anisotropie plastique et application à la mise en forme des tôles métalliques. University of Metz: Metz, 2007

50. Rabahallah M, Balan T, Barlat F. Orthotropic strain rate potentials using multiple linear transformations. *International Journal of Solids and Structures* 2009; **46**:1966–1974.

51. Haddadi H, Bouvier S, Banu M, Maier C, Teodosiu C. Towards an accurate description of the anisotropic behaviour of sheet metals under large plastic deformations: Modelling, numerical analysis and identification. *International Journal of Plasticity* 2006; **22**(12):2226-2271.

52. Chung K, Lee MG, Kim D, Kim C, Wenner ML, Barlat F. Spring-back evaluation of automotive sheets based on isotropic-kinematic hardening laws and non-quadratic anisotropic yield functions: Part I: Theory and formulation. *International Journal of Plasticity* 2005; **21**(5):861-882.

53. Choi Y, Han CS, Lee JK, Wagoner RH. Modeling multi-axial deformation of planar anisotropic elasto-plastic materials, part I: Theory. *International Journal of Plasticity* 2006; **22**(9):1745-1764.

54. Yoshida F, Uemori T. A model of large-strain cyclic plasticity describing the Bauschinger effect and work hardening stagnation. *International Journal of Plasticity* 2002; **18**:661-686.

55. Geng L, Shen Y, Wagoner RH. Anisotropic hardening equations derived from reverse-bend testing. *International Journal of Plasticity* 2002; **18**(5-6):743-767.

56. Teodosiu C (ed.). Large Plastic Deformation of crystaline aggregates. *CISM courses and lectures*, 376, 1997, ISBN 3-211-82909.

57. Teodosiu C, Hu Z. Evolution of the intragranular microstructure at moderate and large strains: Modeling and computational significance. *Simulation of Materials Processing: Theory, Methods and Applications Numiform'95 Proceedings*, 1995; 173-182.

58. Haddag B, Balan T, Abed-Meraim F. Investigation of advanced strain-path dependent material models for sheet metal forming simulations. *International Journal of Plasticity* 2007; **23**(6):951-979.

59. Alves JL. Simulação numérica do processo de estampagem de chapas metálicas: Modelação mecânica e métodos numéricos. University of Minho: Portugal, 2003

60. *Abaqus Version 6.7 Documentation, Dassault Systèmes Simulia Corp.*, 2007.

61. Rabahallah M, Bouvier S, Balan T, Bacroix B. Numerical simulation of sheet metal forming using anisotropic strain-rate potentials. *Materials Science & Engineering A* 2009:accepted.